# Vacancy concentration in Al from combined first-principles and model potential calculations

Karin M. Carling and Göran Wahnström
*Department of Applied Physics, Chalmers University of Technology and Göteborg University, SE-412 96 Göteborg, Sweden*

Thomas R. Mattsson
*Surface and Interface Science Department, MS 1415, Sandia National Laboratories, Albuquerque, New Mexico 87185-1415*

Nils Sandberg and Göran Grimvall
*Theory of Materials, Department of Physics, Royal Institute of Technology, Alba Nova, SE-106 91 Stockholm, Sweden*
(Received 30 September 2002; published 5 February 2003)

We present a comprehensive study of vacancy formation enthalpies and entropies in aluminum. The calculations are done in the framework of the local-density and generalized-gradient approximations in the density-functional formalism. To assess anharmonic contributions to the formation free energies, we use an interatomic potential with parameters determined from density-functional-theory calculations. We find that the binding energy for the nearest-neighbor divacancy is negative, i.e., it is energetically unstable. The entropy contributions slightly stabilize the divacancy but also the binding free energy at the melting temperature is found to be negative. We show that the anharmonic atomic vibrations explain the non-Arrhenius temperature dependence of the vacancy concentration in contrast to the commonly accepted interpretation of the experimental data in terms of the monovacancy-divacancy model.

DOI: 10.1103/PhysRevB.67.054101 PACS number(s): 61.72.Ji, 71.15.−m, 61.72.Bb

## I. INTRODUCTION

Vacancies are the simplest lattice defects and play an important role for various properties of materials, such as kinetic, thermodynamic, electrical, optical, and mechanical properties.[1] One example is mass transport in close-packed structures, where diffusion by vacancies is the most important mechanism.[2] Many of the material properties depend directly on the concentration of vacancies.

There are a number of methods for measurements of the concentration of vacancies in metals.[1,3] At high temperatures, accurate values of the absolute vacancy concentration at equilibrium can be obtained by differential dilatometry.[4–6] For intermediate temperatures, vacancies in equilibrium can be probed by positron annihilation techniques.[7] By combining these two methods,[4,5] the vacancy concentration has become detectable over a large temperature range, about 500 K for Al, corresponding to concentrations varying by more than three orders of magnitude. Another technique, rapid quenching from high temperatures and subsequent investigation of the residual electrical resistance, has also been used extensively.[8]

For many metals, the vacancy concentration shows a curvature when the logarithm of the concentration is plotted against the inverse temperature, i.e., an Arrhenius plot. This curvature is seen in the high-temperature end, when the plot is covering an extended temperature range. Similar behavior is obtained for the temperature dependence of self-diffusion. The commonly accepted interpretation of the curvature is in terms of the monovacancy-divacancy model[9,10] and several experimental studies have been performed to extract the binding energy for the divacancy.[8,11–15] However, it has been proposed that temperature-dependent monovacancy energies could equally well explain the curvature of the Arrhenius plot[16] and that this effect should be considered for fcc metals.[17]

Calculations independent of experimental data, i.e., first-principles calculations, can play an important role in improving the understanding of physical phenomena. We have used this approach to calculate key thermodynamic properties of vacancies and divacancies in Al. The density-functional theory[18,19] (DFT) is widely used together with the nonempirical local-density (LDA) and generalized-gradient (GGA) approximations for the exchange-correlation energy. The theory provides detailed information and can give a better insight on defect-related materials properties. Previously, vacancies in aluminum have been studied using the pseudopotential[20–27] method, the full-potential linearized augmented plane-wave,[28] LMTO (linear muffin-tin orbital),[29] and KKR (Korringa-Kohn-Rostoker)[30,31] methods, and the full-charge density[32] technique.

Mainly static properties of monovacancies have been calculated with the DFT/LDA. An *ab initio* calculation of vibrational properties for the monovacancy can be found in Ref. 23. Calculations of divacancy properties are rare[26,27] and only a few studies employing the GGA have been reported.[27,30,31]

The purpose of the present work is to study divacancies in Al at finite temperatures using *ab initio* based calculational methods. We use the DFT together with *ab initio* based atomistic model potentials. In a previous paper,[27] we presented some computational results for vacancies in Al. Here, we add information on the entropy of formation for both monovacancies and divacancies as well as on the temperature dependences arising from anharmonicity. We analyze the screening of the monovacancy and the binding properties of the divacancy in more detail. We determine from first principles the Gibbs free energy of formation for the monovacancies and divacancies and the vacancy concentration as a function of

 

temperature. Also, we analyze in detail the relative contributions from the enthalpy and entropy of binding to the divacancy concentration.

In Sec. II, we give the appropriate thermodynamic expressions for the defect parameters. The computational methodology is presented in Sec. III and the results for the energy of formation, divacancy binding energy, entropy of formation, and anharmonic contributions are all presented in Sec. IV. In Sec. V, the obtained theoretical results are compared with available experimental data and finally, in Sec. VI, we summarize our conclusions.

## II. THERMODYNAMICS OF DEFECT PARAMETERS

In thermal equilibrium, the vacancy concentration $c_{\mathrm{V}}$ is obtained by minimizing the Gibbs free energy for the defect-containing crystal.[33] In the dilute solution approximation, the total vacancy concentration can be written as a sum of the contribution from monovacancies and divacancies according to

$$c_{\mathrm{V}} = c_{1\mathrm{V}} + 2c_{2\mathrm{V}} = e^{-G^{\mathrm{F}}_{1\mathrm{V}}/k_{\mathrm{B}}T} + 2g_{2\mathrm{V}}e^{-G^{\mathrm{F}}_{2\mathrm{V}}/k_{\mathrm{B}}T} = c_{1\mathrm{V}} + 2g_{2\mathrm{V}}c_{1\mathrm{V}}^2 e^{G^{\mathrm{B}}_{2\mathrm{V}}/k_{\mathrm{B}}T}, \quad (1)$$

where $g_{2\mathrm{V}}=6$ for nearest-neighbor divacancies in the fcc lattice. The Gibbs free energy of formation can be decomposed into the the enthalpy and entropy of formation,

$$G^{\mathrm{F}}_{X\mathrm{V}}(T,P) = H^{\mathrm{F}}_{X\mathrm{V}}(T,P) - TS^{\mathrm{F}}_{X\mathrm{V}}(T,P). \quad (2)$$

The notation $G^{\mathrm{F}}_{X\mathrm{V}}$ is used for $G^{\mathrm{F}}_{1\mathrm{V}}$ and $G^{\mathrm{F}}_{2\mathrm{V}}$, and correspondingly for the other thermodynamic quantities. We will restrict our analysis to constant pressure ($P=0$) and the dependence on $P$ will be dropped throughout the paper. The enthalpy is then equal to the energy, since at atmospheric pressure the $PV$ term is negligible, $H \gg PV$.

In the harmonic approximation, at sufficiently high temperatures where quantum effects in the atomic vibrational motion can be neglected, the enthalpy and entropy of formation are given by

$$H^{\mathrm{F}}_{X\mathrm{V}}(T) = H^{\mathrm{F}}_{X\mathrm{V}}(T=0) \quad (3)$$

and

$$S^{\mathrm{F}}_{X\mathrm{V}}(T) = k_{\mathrm{B}}\sum_i \ln(\omega_i^0/\omega_i^{X\mathrm{V}}), \quad (4)$$

where $\omega_i^{X\mathrm{V}}$ and $\omega_i^0$ denote the harmonic frequencies for the crystal with and without vacancies, respectively. The entropy of formation is therefore positive if, on the average, the frequencies are lowered when creating a vacancy. Notice that in the harmonic approximation, both the enthalpy and entropy of formation are temperature independent. We denote these quantities $H^{\mathrm{F}}_{1\mathrm{V}}$, $H^{\mathrm{F}}_{2\mathrm{V}}$, $S^{\mathrm{F}}_{1\mathrm{V}}$, and $S^{\mathrm{F}}_{2\mathrm{V}}$.

With increasing temperature the vibrational motion becomes anharmonic. This may introduce a temperature dependence for the enthalpy of formation

$$H^{\mathrm{F}}_{X\mathrm{V}}(T) \equiv f_{X\mathrm{V}}(T)H^{\mathrm{F}}_{X\mathrm{V}}. \quad (5)$$

According to the thermodynamic relation $(\partial H/\partial T)_P = T(\partial S/\partial T)_P$ the entropy of formation is given by

$$S^{\mathrm{F}}_{X\mathrm{V}}(T) = S^{\mathrm{F}}_{X\mathrm{V}} + H^{\mathrm{F}}_{X\mathrm{V}}\int^T \frac{dT_1}{T_1} f'_{X\mathrm{V}}(T_1). \quad (6)$$

In addition to the vibrational part there is also an electronic contribution to the entropy of formation.[34] However, this contribution is very small[34] and will be neglected in the present paper.

## III. COMPUTATIONAL METHODOLOGY

Different objectives require different approaches and methods. We have therefore performed both the first-principles DFT[18,19] calculations and the interatomic model potential (MP) simulations. The DFT is used to calculate energies and forces for systems of limited size. For large simulations, we resort to the MP.

In the DFT calculations the exchange-correlation energy is treated using two different approximations, the LDA and the GGA by Perdew *et al.*[35] We denote results from these two sets of calculations DFT/LDA and DFT/GGA, respectively.

The plane-wave, pseudopotential method, as implemented in the DACAPO[36] and VASP[37] codes, is used. The formation energies are calculated with DACAPO, and the force constants for the evaluation of the vibrational entropy are calculated with VASP. The calculated formation energies differ 3% for the monovacancy and 6% for the divacancy, at most, between the two codes. Different pseudopotentials[38,39] are used for respective exchange-correlation approximation. The periodic supercells[40] consist of 32–125 lattice sites. The reported numbers are for the 80 lattice-sites cell. The cutoff energy for the plane waves is taken to be $E_{\mathrm{cutoff}}=130$ eV and the Brillouin zone is sampled according to the Monkhorst-Pack method[41] with $4\times4\times4$ $k$ points for the supercell with 80 lattice sites. To improve the $k$ point convergence, the Fermi discontinuity is smoothed using the Gillan scheme[20] with the effective electronic temperature 0.2 eV.

In the MP simulations, we use the interatomic model potential for Al developed by Ercolessi and Adams (EA).[42] The model potential is of the pair-functional form, i.e., it consists of a pair potential in combination with an embedding functional that includes a part of the many-body interaction. In particular, the energy dependence on the coordination number $C$ is roughly proportional to $\sqrt{C}$,[43] making pair functionals much more realistic in modeling metals than pair potentials, which have a linear dependence on coordination.

The parameters in the EA potential are optimized by comparing the results with an extensive set of geometries, e.g., monovacancy and high-temperature geometries, from the first-principles DFT calculations within the LDA.[42] There is no experimental information included in the fitting dataset, the potential, thus, being constructed independently of experimental data. We denote results using the Ercolessi-Adams model potential, the MP/EA. The molecular-dynamics simulations using the EA model potential are done for systems with 500 lattice sites. Constant temperature and

TABLE I. The enthalpy of formation for the monovacancy ($H^F_{1V}$) and the divacancy ($H^F_{2V}$), and the binding energy ($H^B_{2V} \equiv 2H^F_{1V} - H^F_{2V}$) for the divacancy from the DFT calculations with the LDA and the GGA, and from the EA model potential.

| | $H^F_{1V}$ (eV) | | $H^F_{2V}$ (eV) | | $H^B_{2V}$ (eV) | |
|---|---|---|---|---|---|---|
| | Unrelax | Relax | Unrelax | Relax | Unrelax | Relax |
| LDA | 0.78 | 0.70 | 1.62 | 1.48 | -0.07 | -0.07 |
| GGA | 0.63 | 0.55 | 1.33 | 1.19 | -0.07 | -0.08 |
| EA | | 0.69 | | 1.38 | | 0.01 |
| Expt., Ref. 53 | $0.67 \pm 0.03$ | | | | $0.25 \pm 0.05$ | |

(zero) pressure conditions are achieved using the Hoover and Parrinello-Rahman algorithms.[44] A typical simulation covers about 20–40 ns.

## IV. THEORETICAL RESULTS

### A. Energy of formation

A vacancy introduces two effects: a region with low electron density and relaxation of the atomic positions. The former effect dominates the vacancy formation energy, while relaxation contributes with a minor, but not negligible, part.[45] The energy of formation in a supercell geometry is

$$H^F_{XV} = E(N-X, V_X) - \frac{N-X}{N} E(N,V), \tag{7}$$

where $X$ is the number of vacancies and $E(N,V)$ the total energy for $N$ atoms at volume $V$. In the defect calculations, we allow for both atom and volume relaxation. This corresponds to the boundary condition of constant pressure ($P=0$). One can also perform the calculations at constant volume. The results from both methods converge to the correct defect energy, when the size of the supercell is increased.[46] The periodic cell must be large enough to make the interaction between defects negligible. A straightforward convergence test using $N=32$, 64, 108, and 125 shows that the energy of formation is converged to 0.01 eV for $N=80$.[47]

Resulting formation energies are given in Table I. The GGA values are lower than the energies in the LDA for both monovacancies and divacancies. The differences are significant compared to other energies, showing that the choice of exchange-correlation functional is important in the calculation. The difference is the same for the unrelaxed and relaxed cases, implying that the effect has electronic origin and is independent of the structural relaxation.

The local reduction of the electron density is substantial in the vacancy.[27] It is reduced from its bulk value $\bar{n} = 0.18$ Å$^{-3}$, becoming close to zero, 0.02 Å$^{-3}$, at the vacancy center. This rapid and large decrease of the electron density is very similar to the behavior at a surface,[27] suggesting that we can regard the vacancy as an internal surface. For the generic electron surface, the jellium surface, it is known that the LDA and the GGA both underestimate the magnitude of the surface energy, with GGA showing the largest discrepancy.[48] The difference between the LDA and the GGA in describing the exchange-correlation energy for the jellium surface is consistent with the differences in Table I. Based on the error in the jellium surface energy one can formulate a correction to the vacancy formation energy,[27,45] which is of the order of 0.15 eV (0.06 eV) for GGA (LDA).[27]

A comparison with previously reported results for the monovacancy formation energy show that, for LDA, pseudopotential calculations[24–26] give a formation energy of 0.66 eV, while full-potential calculations[30–32] give an energy in the range from 0.62 eV to 0.73 eV. Previously reported results for the GGA are scarce and range from 0.53 eV to 0.59 eV.[30,31] For both the LDA and the GGA our results are within the range of previously reported results.

The EA model potential is fitted to forces and energies in the LDA. Therefore, the agreement in energy in Table I between the EA and the LDA is expected. In particular, various geometries including the monovacancy are included in the fitting process,[42] resulting in the close agreement for the monovacancy formation energy. Geometries including divacancies are *not* included in the fitting process. The divacancy formation energy is, thus, an assessment of how transferable the MP is. With the EA value for $H^F_{2V}$ being 7% lower than that of the LDA, we conclude that the EA potential describes the divacancy quite well, in terms of the formation energy.

### B. Divacancy binding energy

Using the results for the formation energies, we can analyze the binding properties of the divacancy. The divacancy binding energy is defined as

$$H^B_{2V} \equiv 2H^F_{1V} - H^F_{2V}, \tag{8}$$

where $H^F_{1V}$ is the monovacancy and $H^F_{2V}$ the divacancy formation energy. If the binding energy is positive, it is energetically favorable to form a divacancy from two monovacancies.

From a simple bond model the divacancy binding energy is 1/6 of the monovacancy formation energy due to the fact that fewer bonds are broken when forming the divacancy compared with two monovacancies.[49] Taking into account that, in a metal, the energy per bond decreases with increasing coordination number, the divacancy binding energy should be somewhat less than 1/6 of the monovacancy formation energy. This is also what is found for Cu, Ni, Ag, and Pd.[49,50]

Here, we find a negative binding energy, both using the LDA and the GGA (see Table I). The energy needed to remove an atom, that is, a nearest neighbor to a monovacancy is larger than the energy needed to remove a bulk atom. This is somewhat surprising since there are fewer bonds to break in the former case. However, it is compatible with the DFT/LDA results for the variation of the energy dependence on the coordination number for various Al structures found in Ref. 43. The result is more or less the same for both the DFT/LDA and the DFT/GGA, which is consistent with our conjecture that the error in the formation energy is proportional to the internal surface area. Also, the result is independent of relaxation of the atomic positions.

To gain more insight, we have investigated the effect on the electron density from the vacancy formation. In Fig. 1,

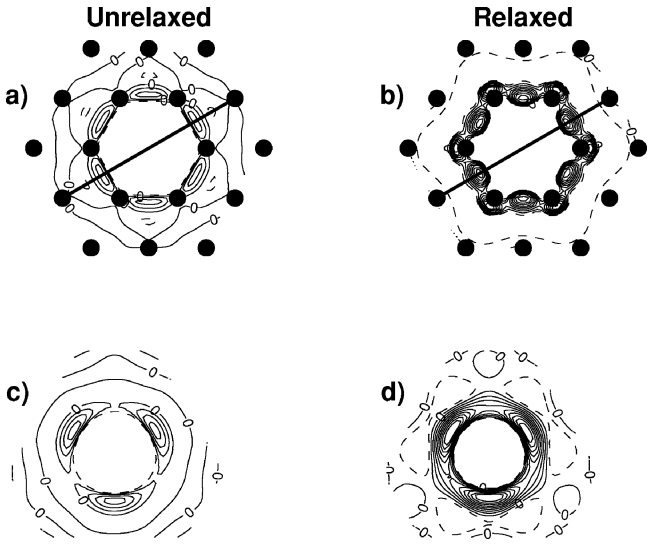


FIG. 1. The charge-density difference between the unrelaxed vacancy and bulk (left), and relaxed vacancy and bulk (right). In all figures the cut is parallel to the [111] plane. In (a) and (b) the cut is through the vacancy (vacancy plane), and the line indicates the direction of the density plot in Fig. 3. In (c) and (d) the cut is the plane half-way between the atom planes (half-way plane). Solid lines show charge-density increase contours. The difference between two consecutive contour-lines is 0.002 eV/Å$^3$. Dashed line show the $-0.002$ eV/Å$^3$ contour.

we show the induced increase of the electron density when a single monovacancy has been formed. The difference in electron density between the perfect bulk and the monovacancy systems is more or less negligible for the regions beyond the first shell. The vacancy is efficiently screened, as has been found previously.[21,29] Each atom in the first shell has four in-shell nearest neighbors. The increase in the induced electron density is concentrated to the regions between in-shell nearest neighbors, the ''triangles'' in Fig. 2. This is clearly seen in Figs. 1(c) and 1(d), where the induced electron density is shown in a plane half-way between the [111] planes. The increase is present for both the unrelaxed and relaxed systems. However, it is larger for the relaxed system, by a factor of 3. A similar effect was found for the Al(110) surface.[51] We also show the total densities in Fig. 3. They are shown along the line indicated in Figs. 1(a) and 1(b). The inward shift in the charge density towards the vacancy center for the relaxed system is mainly due to the atomic relaxation. The atoms in the first shell are displaced 0.05 Å towards the vacancy center.

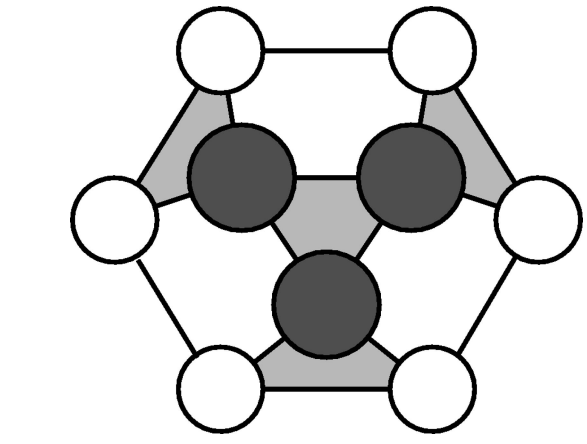

FIG. 2. The geometry of the atoms being nearest neighbors to the vacancy (first-shell atoms, nine of twelve atoms are shown). Each atom has four in-shell nearest neighbors. These atoms are geometrically connected though triangles (four of eight of these triangles are shown, in gray).

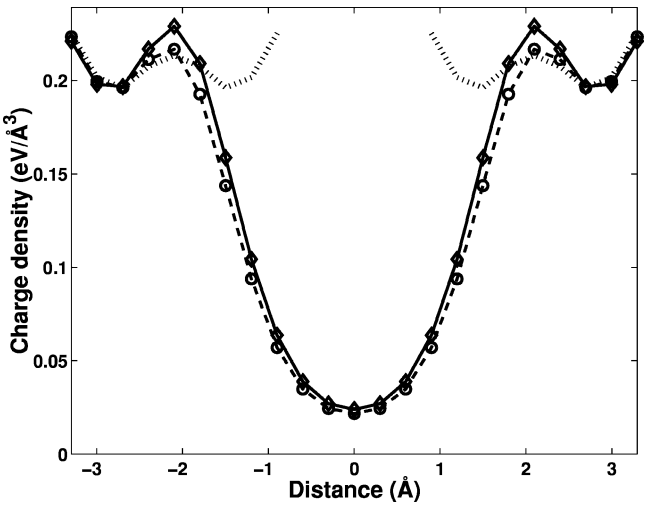


FIG. 3. The total densities along the lines shown in Fig. 1. Dashed line with circles: density for the unrelaxed vacancy, Fig. 1(a). Solid line with diamonds: density for the relaxed vacancy, Fig. 1(c). Dotted line: bulk density outside pseudopotential cutoff radius. The density is equal to the bulk density 2.6 Å from the vacancy center.

We have also investigated the changes in the different components of the force-constant matrix $\phi_{i,j}^{\alpha,\beta} \equiv m D_{i,j}^{\alpha,\beta}$, where the dynamical matrix $D_{i,j}^{\alpha,\beta}$ is defined in Eq. (9) and $m$ is the mass of the Al atoms. In bulk Al, all three eigenvalues of the diagonal elements of the force-constant matrix $\phi_{i,i}^{\alpha,\beta}$ are equal to 4.42 eV/Å$^2$. When the monovacancy is formed, the diagonal elements become 4.96 eV/Å$^2$, 4.74 eV/Å$^2$, and 3.42 eV/Å$^2$ for the atoms in the first shell. The lowest eigenvalue corresponds to the direction towards the vacancy center. For atoms in the second shell, the changes are considerably smaller and the eigenvalues are equal to 4.50 eV/Å$^2$, 4.49 eV/Å$^2$, and 4.33 eV/Å$^2$. In addition, we have analyzed the matrix elements $\phi_{i,j}^{\alpha,\beta}$ that couple nearest-neighbor atoms $i$ and $j$ in the first shell around the vacancy. The largest eigenvalue, corresponding to the coupling along the line joining the two atoms, is increased from its bulk value 1.15 eV/Å$^2$ to 1.45 eV/Å$^2$, i.e., an increase by 25%. These results show that many-body effects are present and the bonding is modified substantially when the vacancy is formed.

It is interesting to compare the DFT/LDA values with the result using the interatomic model potential. In the latter case, the binding energy is found to be slightly positive. The model potential gives a good account of the formation energy of the monovacancy but the divacancy energy is too

small. This is not surprising. Configurations with monovacancies were included in the fitting procedure and the difference in energy for the divacancy is within the accuracy that is expected for pair-functional models for Al.[43] It demonstrates the difficulty in modeling the details of the interatomic interaction, in particular, if the coordination is changing and the electron density is redistributed.

### C. Entropy of formation

The entropy of formation is obtained in the harmonic approximation by evaluating the dynamical matrix

$$D_{i,j}^{\alpha,\beta}=\frac{1}{m}\frac{\partial^2 E}{\partial u_i^{\alpha}\partial u_j^{\beta}}, \tag{9}$$

for both perfect and defect containing systems. $E$ is the total energy of the system, and $u_i^{\alpha}$ and $u_j^{\beta}$ the displacements of atoms $i$ and $j$ in directions $\alpha$ and $\beta$ from their relaxed equilibrium positions.

The calculations are performed for a supercell with the boundary condition of constant pressure ($P=0$). The dynamical matrix is determined by displacing the atoms $\pm 0.05$ Å in all three different directions. The distance 0.05 Å is sufficient to get accuracy in evaluating the derivatives numerically and small enough to be in the harmonic region.

The dynamical matrix is diagonalized and the eigenfrequencies $\omega_i$ are determined. The entropy is then evaluated from the expression

$$S_{XV}^{F}=-k_B\left[\sum_{i=1}^{3(N-1-X)}\ln\omega_i^{XV}-\frac{N-1-X}{N-1}\sum_{i=1}^{3(N-1)}\ln\omega_i^{0}\right], \tag{10}$$

where we have taken into account that three eigenvalues of the dynamical matrix are zero due to the translational invariance of the system.

The DFT calculations of the dynamical matrix for a reasonably large system are very demanding, and we have instead performed MP calculations for system sizes of several hundred atoms. We find a system size of 500 lattice points to be sufficient to get well-converged values. For the monovacancies and divacancies, we get $S_{1V}^{F}=1.31k_B$ and $S_{2V}^{F}=1.97k_B$, respectively.

To assess the accuracy of the entropy calculations, we have also performed the DFT calculations for two different smaller systems. These two systems give an upper(''$u$'') and lower(''$l$'') limit, respectively, for the entropy of formation.

In the first case, we have considered an embedded-cluster calculation.[34,46] Only the atoms in the first shell around the vacancy are considered as dynamic, and only their vibrations are taken into account in the calculation of the entropy. This corresponds to 13, 12, and 18 dynamic atoms for the perfect bulk, monovacancy and divacancy calculations, respectively. The size of the supercell is in all cases 80 atoms. We denote this case with an ''$u$.'' The corresponding entropy is larger compared with the correct value. In the limit of relatively small embedded clusters, or relatively large supercells, the entropy converges to the defect core entropy, which is larger than the correct value.[46]

TABLE II. The entropy of formation for the monovacancy ($S_{1V}^{F}$) and the divacancy ($S_{2V}^{F}$), together with the result for the binding entropy $S_{2V}^{B}\equiv 2S_{1V}^{F}-S_{2V}^{F}$. Results from two different small systems are indicated by ''$-l$'' and ''$-u$,'' and they give lower ($l$) and upper ($u$) limits for the entropy of formation. The EA result is for a large system while the LDA and GGA results are based on the result for the two smaller systems. For more details see Sec. IV C.

| Method | $S_{1V}^{F}$ ($k_B$) | $S_{2V}^{F}$ ($k_B$) | $S_{2V}^{B}$ ($k_B$) |
|---|---|---|---|
| EA-l | 1.19 | 1.34 | 1.04 |
| EA-$u$ | 1.44 | 2.45 | 0.43 |
| LDA-l | 0.76 | 1.66 | -0.13 |
| LDA-$u$ | 1.03 | 2.45 | -0.39 |
| GGA-l | 0.65 | 1.40 | -0.10 |
| GGA-$u$ | 0.94 | 2.18 | -0.31 |
| EA | 1.31 | 1.97 | 0.64 |
| LDA | 0.9 | 2.1 | -0.3 |
| GGA | 0.8 | 1.8 | -0.2 |
| Expt., Ref. 53 | 0.7 | | |

In the second case, we consider the same embedded cluster geometry. However, we do not include all elements in the dynamical matrix, only the diagonal terms $D_{i,i}^{\alpha,\beta}$. This corresponds to the Einstein approximation, or the local harmonic approximation. It gives a lower value compared with the correct value.[46] We denote it with an ''$l$.''

We have also performed the MP calculations for the same two simplified systems (but with a supercell of 500 lattice points). In Table II, we give our results. Indeed, we find from the MP calculations that the two simplified models give a lower and an upper bound for the correct entropy of formation. We can therefore get a better approximation from the DFT calculations by taking a weighted average of the DFT-l and DFT-$u$ numbers. We obtain the values $S_{1V}^{F}=0.9k_B$, $S_{2V}^{F}=2.1k_B$, and $S_{1V}^{F}=0.8k_B$, $S_{2V}^{F}=1.8k_B$, for the LDA and the GGA, respectively. In the same table, we also give the binding entropies[52]

$$S_{2V}^{B}\equiv 2S_{1V}^{F}-S_{2V}^{F}. \tag{11}$$

The difference in the entropy of formation between the LDA and the GGA is small, both for the monovacancies and divacancies. We expect the weighted averaged values to be rather good approximations for the true DFT numbers. The binding entropies are slightly negative, which implies that the divacancy is stabilized by the entropy contribution. However, the effect is small. At 500 K the addition is only 0.01 eV to the divacancy binding free energy, considerably less than the (negative) enthalpy contribution.

The EA number for the monovacancy deviates from the DFT numbers, despite the fact that the EA model has been fitted to the DFT/LDA values. The difference becomes apparent for the binding entropy. Again, it illustrates the limitation of a pair-functional model potential to capture the details of the interatomic interaction close to a vacancy in Al.

### D. Anharmonic contributions

When the temperature is increased, anharmonic contributions to the lattice vibrations become important. One part of this effect can be described by the quasiharmonic approximation but at high temperatures, close to the melting temperature, the explicit anharmonicity due to the increased vibrational amplitudes has to be taken into account. A large number of configurations contribute and the DFT calculations become very expensive. We have therefore used MP simulations to determine the anharmonic effect. Note that high-temperature geometries are included in the fitting process of the EA potential, ensuring that the anharmonic behavior is a part of this potential.

The temperature dependence in Eq. (5) can be obtained by comparing the energy of the perfect bulk system with that of a defect containing system as a function of temperature. We have performed molecular-dynamics simulations at constant temperature and constant (zero) pressure. At each temperature the production part of the simulation run covers of the order of 20–40 ns, but up to 80 ns trajectories were used. In all cases, we use a system with 500 lattice points.

For the monovacancy calculations, we remove one atom. The system is allowed to evolve in time and the monovacancy samples different configurations. It can also diffuse. It is possible that new defects are formed in the simulation, such as an interstitial-vacancy pair. We have monitored the atomic positions and no such events have been detected.

In the divacancy case, we remove two nearest-neighbor atoms. Different configurations are sampled and only those that can be characterized as a nearest-neighbor divacancy are included. The divacancy may diffuse. After the diffusive event it can still be a nearest-neighbor divacancy but it can also split into two monovacancies (a second nearest-neighbor divacancy). To avoid the latter event, we have monitored continuously the reaction coordinates $\xi_i=[\mathbf{R}_i-1/4\Sigma_{j=1}^{4}\mathbf{R}_j]\cdot\mathbf{e}_i$, where $\mathbf{R}_i$ denotes the position of the atom in question and $\mathbf{R}_j$ the four atoms that constitute the ''bottle neck'' of the jump into the vacant site. The vector $\mathbf{e}_i$ is a unit vector in the direction $\mathbf{R}_i$. When any $\xi_i$ exceeded zero, it was reflected back by applying a harmonic restoring force. The barrier for divacancy splitting was calculated to be 0.675 eV for the EA potential, i.e., slightly higher than the vacancy migration barrier.[47] Taking for the prefactor the value for vacancy migration, one finds that, at $T=900$ K, ''attempts to split'' will occur with an average interval of 20 ps, In the actual simulation an interval of 10 ps was found. Since the procedure of reflecting unwanted jumps takes about 20 fs, the effect on the calculated value of $H_{2V}^{F}(T)$ is negligible.

In Fig. 4, we present our results for the temperature dependences of enthalpy of formation for the monovacancies and divacancies. We have fitted the result to a polynomial. The entropy of formation can then be obtained according to Eq. (6) and the Gibbs free energy from Eq. (2). Using the LDA(GGA) numbers $H_{1V}^{F}=0.70(0.55)$ eV, $H_{2V}^{F}=1.48(1.19)$ eV and $S_{1V}^{F}=0.9(0.8)k_B$, $S_{2V}^{F}=2.1(1.8)k_B$, we get the data in Table III at the melting temperature $T_m=933$ K.

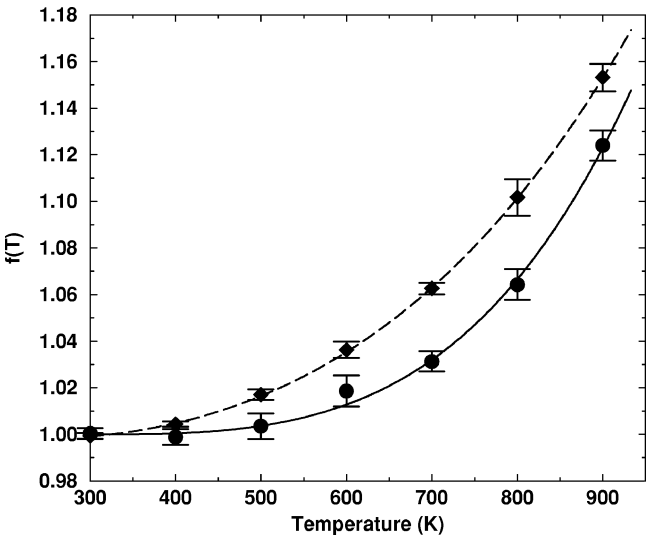


FIG. 4. The temperature dependence of the monovacancy and divacancy enthalpy of formation. The molecular-dynamics simulation results for $f(T)$, see Sec. II, are the circles (monovacancy) and the diamonds (divacancy). The lines show the polynomial fit that is used when calculating the vacancy concentration with anharmonicity included.

We find that the binding free energy for the divacancy is equal to $G_{2V}^{B}(T_m)=-0.13(-0.13)$ eV for LDA(GGA). The anharmonicity makes the divacancy even more unstable. Neglecting the anharmonic contribution, we get $G_{2V}^{B}=-0.06$ $(-0.07)$ eV at the melting temperature.

## V. COMPARISON WITH EXPERIMENTAL DATA

Monovacancies have been studied extensively in the past and an excellent compilation of experimental data can be found in Landolt-Börnstein.[53] Our calculated DFT/LDA value is consistent with the experimental results ($H_{1V}^{F}=0.67\pm0.03$ eV, see Table I), while the DFT/GGA value is too low. As already stated, a likely reason for the low DFT/GGA numbers is the inability of the GGA to treat the (jellium) surface accurately. The low DFT/GGA numbers for the energy of formation are reported for other elements for both full-potential[31] and pseudopotential[45] calculations. We argue that both the DFT/GGA and the DFT/LDA numbers should be corrected, but the correction is smaller for the DFT/LDA.[27]

The recommended[53] experimental number for the entropy of formation is $S_{1V}^{F}=0.7k_B$. Our calculated DFT numbers are surprisingly close to the experimental value (see Table

TABLE III. The enthalpy, entropy, and Gibbs free energy of formation at the melting temperature $T_m=933$ K. The temperature dependence has been determined from the EA model potential.

| | $H_{1V}^{F}$ (eV) | $S_{1V}^{F}$ ($k_B$) | $H_{2V}^{F}$ (eV) | $S_{2V}^{F}$ ($k_B$) | $G_{1V}^{F}$ (eV) | $G_{2V}^{F}$ (eV) |
|---|---|---|---|---|---|---|
| LDA | 0.78 | 1.6 | 1.74 | 3.8 | 0.65 | 1.43 |
| GGA | 0.61 | 1.3 | 1.40 | 3.1 | 0.51 | 1.15 |

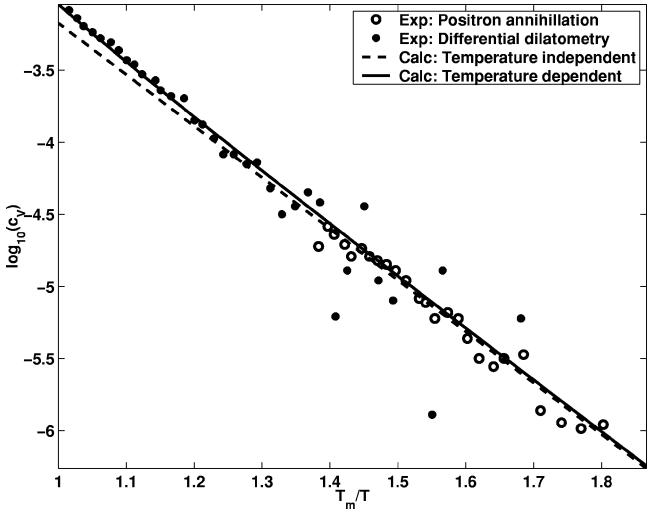


FIG. 5. The vacancy concentration $c_V(T)$ as function of the inverse temperature ($T_m = 933$ K). The experimental positron annihilation (open circles) and differential dilatometry (filled circles) data are taken from Ref. 5. The dashed line shows the result with temperature-independent enthalpies of formation. The DFT/LDA numbers are used but the value for $H^F_{1V}$ is adjusted to $H^F_{1V} = 0.66$ eV to fit the experimental data. The solid line shows the result with temperature-dependent enthalpies of formation and with $H^F_{1V} = 0.66$ eV. The calculated temperature dependence of the formation enthalpies explains the curvature at the high temperature.

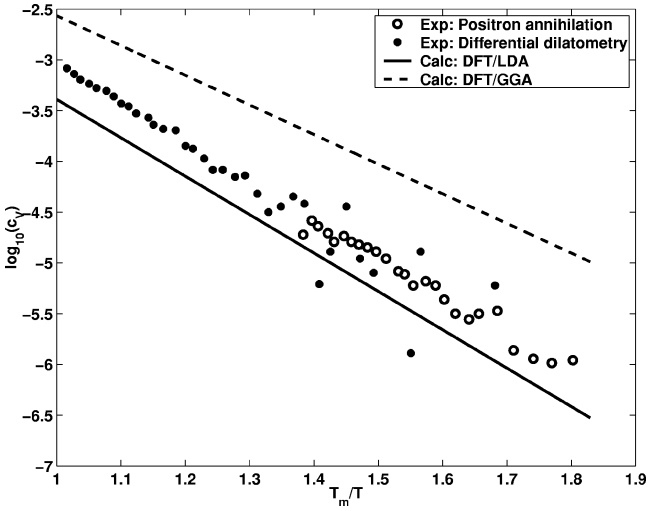


FIG. 6. The vacancy concentration $c_V(T)$ as function of the inverse temperature ($T_m = 933$ K). The experimental positron annihilation (open circles) and differential dilatometry (filled circles) data are taken from Ref. 5. The solid and dashed lines show the result from the DFT/LDA and the DFT/GGA, respectively, without making any adjustments of the calculated results. The deviations from the experimental data are caused by the LDA overestimating and GGA underestimating the value for $H^F_{1V}$ (cf. Fig. 5).

II). Both the DFT/LDA and the DFT/GGA numbers agree with experiments within experimental uncertainties.

For the divacancy, the binding energy from calculations is inconsistent with the experimental number, if the monovacancy-divacancy model is used in analyzing the experiments. We find a repulsive binding energy, in marked contrast to the commonly accepted experimental result of an attractive binding energy (Table I). The calculated value of the divacancy binding entropy gives a positive contribution to the free energy, but considerably smaller when compared with the magnitude of the divacancy binding energy.

The monovacancy-divacancy interpretation of experimental data assumes temperature-independent formation enthalpies. If we relax this assumption we find that our calculated temperature dependence for the formation enthalpies can explain the curvature at the high-temperature end of the experimental data. This is illustrated in Fig. 5. In that figure, we compare our results with the experimental results from Ref. 5. We have then used the DFT/LDA numbers from Table I and Table II, but adjusted the value for $H^F_{1V}$ to fit the experimental data. The temperature dependence is taken from the data in Fig. 4. The calculated result agrees equally well with experimental data, with or without including the contribution from divacancies.

Finally, we make a comparison, in Fig. 6, without making any adjustments of the calculated results. The DFT numbers are taken from Table I and Table II and the temperature dependence is evaluated from the data given in Fig. 4. We have included both monovacancy and divacancy data in the evaluation of the vacancy concentration, even though the divacancy contribution is four orders of magnitude smaller than the monovacancy contribution at the melting point. The calculated results agree with experiments within a factor of 3 at the melting temperature.

## VI. CONCLUSIONS

The Gibbs free energy of formation of monovacancies and divacancies in Al has been determined as a function of temperature by combining the DFT calculations with atomistic simulations. The DFT calculations are performed both using the LDA and the GGA by Perdew *et al.*[35] The interatomic potential, used in the atomistic simulations, has been determined by fitting to first-principles DFT data[42] making our modeling independent of experimental results. A detailed comparison with available measurements[5] of the absolute vacancy concentration is performed.

We find that the largest uncertainty in the free energy of formation comes from the approximation of the exchange-correlation functional in the DFT. The LDA and the GGA by Perdew *et al.*[35] give results that differ by about 25% for the enthalpy of formation at low temperatures. We argue that it is due to the surface effects that are not treated properly. Based on the error in the jellium surface energy, we expect both the LDA and, in particular, the GGA number for the vacancy formation energy to be too low. Improved approximations for the exchange-correlation functional are required in accurate calculations of the vacancy formation energies in metals.

The binding energy for the divacancy is found to be negative, i.e., it is energetically favorable to form two monovacancies from a divacancy. This is in contrast to what has been found from the DFT calculations for Cu, Ni, Ag, and Pd,[49,50] but compatible with the DFT/LDA results[43] for the variation of the energy dependence on the coordination num-

ber for various Al structures. The result is more or less equal for both the DFT/LDA and the DFT/GGA, which is consistent with our conjecture that the error in the formation energy is proportional to the internal surface area.

The harmonic contribution to the entropy of formation is found to agree with experimental data, and both the LDA and the GGA give very similar results. It gives a small positive contribution to the binding free energy of the divacancy and makes it slightly less unstable.

Furthermore, we show that our calculated temperature dependence for the formation energies is sufficient to explain the curvature at the high-temperature end of the experimental data. Divacancies are not required in order to understand the experimental result for Al. The predictability of the atomistic simulations is not as high as that of the direct DFT calculations, but the conclusion, that the temperature dependence has to be included in a detailed analysis of experimental data, is well founded. The anharmonicity is shown to give a negative contribution to the binding free energy and makes the divacancy somewhat more unstable.

In conclusion, we have found that the nearest-neighbor divacancy binding energy in Al is negative (repulsive interaction), and we show that the temperature dependence of the enthalpy of formation, caused by anharmonicity of the lattice vibrations, explains the curvature at the high-temperature end of the experimental data for Al. This is in contrast to recent analysis of experimental data,[8,15] where temperature-independent formation energies are assumed and a positive binding energy (attractive interaction) for the divacancy is deduced.

## ACKNOWLEDGMENTS

We thank A. E. Mattsson and T. Hehenkamp for helpful discussions. This work was supported by the Swedish organizations VR, SSF, and NGSSC. K.M.C. acknowledges the received computer time on the IBM SP2 machine at PDC in Stockholm. T.R.M. acknowledges support from the Motorola/SNL computational materials CRADA. Sandia is a multiprogram laboratory operated by Sandia Corporation, a Lockheed Martin Company, for the United States Department of Energy under Contract No. DE-AC04-94AL85000.

[1] H.J. Wollenberger, in *Point Defects*, 4th ed., edited by R.W. Cahn and P. Haasen, Physical Metallurgy, Vol. 2 (Elsevier Science BV, Amsterdam, The Netherlands, 1996), Chap. 18.
[2] J.L. Bocquet, G. Brebec, and Y. Limoge, in *Diffusion in Metals and Alloys*, 4th ed., edited by R.W. Cahn and P. Haasen, Physical Metallurgy, Vol. 1 (Elsevier Science BV, Amsterdam, The Netherlands, 1996), Chap. 7.
[3] Y. Kraftmakher, Phys. Rep. **299**, 79 (1998).
[4] J.-E. Kluin, Philos. Mag. A **65**, 1263 (1992).
[5] T. Hehenkamp, J. Phys. Chem. Solids **55**, 907 (1994).
[6] R.W. Cahn, Nature (London) **397**, 656 (1999).
[7] M.J. Fluss, S. Berko, B. Chakraborty, K.R. Hoffmann, P. Lippel, and R.W. Siegel, J. Phys. F: Met. Phys. **14**, 2831 (1984).
[8] A. Khellaf, A. Seeger, and R.M. Emrick, Metall. Trans. **43**, 186 (2002).
[9] A. Seeger and H. Mehrer, in *Vacancies and Interstitials in Metals*, edited by A. Seeger, D. Schumacher, W. Schilling, and J. Diehl (North-Holland, Amsterdam, 1970), p. 1.
[10] A. Seeger, D. Wolf, and H. Mehrer, Phys. Status Solidi B **48**, 481 (1971).
[11] R.W. Balluffi, J. Nucl. Mater. **69/70**, 240 (1978).
[12] V. Levy, J.M. Lanore, and J. Hillairet, Philos. Mag. **28**, 373 (1973).
[13] M. Doyama and J.S. Koehler, Phys. Rev. **134**, A522 (1964).
[14] M.J. Fluss, S. Berko, B. Chakraborty, P. Lippel, and R.W. Siegel, J. Phys. F: Met. Phys. **14**, 2855 (1984).
[15] G. Neumann, V. Tölle, and C. Tuijn, Physica B **271**, 21 (1999).
[16] H.M. Gilder and D. Lazarus, Phys. Rev. B **11**, 4916 (1975).
[17] J.N. Mundy, Phys. Status Solidi B **144**, 233 (1987).
[18] P. Hohenberg and W. Kohn, Phys. Rev. **136**, B864 (1964).
[19] W. Kohn and L.J. Sham, Phys. Rev. **140**, A1133 (1965).
[20] M.J. Gillan, J. Phys.: Condens. Matter **1**, 689 (1989).
[21] A. De Vita and M.J. Gillan, J. Phys.: Condens. Matter **3**, 6225 (1991).
[22] R. Benedek, L.H. Yang, C. Woodward, and B.I. Min, Phys. Rev. B **45**, 2607 (1992).
[23] A. Caro, D.A. Drabold, and O.F. Sankey, Phys. Rev. B **49**, 6647 (1994).
[24] N. Chetty, M. Weinert, T.S. Rahman, and J.W. Davenport, Phys. Rev. B **52**, 6313 (1995).
[25] D.E. Turner, Z.Z. Zhu, C.T. Chan, and K.M. Ho, Phys. Rev. B **55**, 13 842 (1997).
[26] M.I. Baskes, M. Asta, and S.G. Srinivasan, Philos. Mag. A **81**, 991 (2001).
[27] K. Carling, G. Wahnström, T.R. Mattsson, A.E. Mattsson, N. Sandberg, and G. Grimvall, Phys. Rev. Lett. **85**, 3862 (2000).
[28] M.J. Mehl and B.M. Klein, Physica B **172**, 211 (1991).
[29] H.M. Polatoglou, M. Methfessel, and M. Scheffler, Phys. Rev. B **48**, 1877 (1993).
[30] T. Hoshino, N. Papanikolaou, R. Zeller, P.H. Dederichs, M. Asato, T. Asada, and N. Stefanou, Comput. Mater. Sci. **14**, 56 (1999).
[31] T. Hoshino, T. Mizuno, M. Asato, and H. Fukushima, Metall. Trans. **42**, 2206 (2001).
[32] L. Vitos, Phys. Rev. B **64**, 014107 (2001).
[33] G. Grimvall, *Thermophysical Properties of Materials* (Elsevier, Amsterdam, 1999).
[34] R.D. Hatcher, R. Zeller, and P.H. Dederichs, Phys. Rev. B **19**, 5083 (1979).
[35] J.P. Perdew, J.A. Chevary, S.H. Vosko, K.A. Jackson, M.R. Pederson, D.J. Singh, and C. Fiolhais, Phys. Rev. B **46**, 6671 (1992); **48**, 4978(E) (1993).
[36] L. Hansen *et al.*, Center for Atomic Scale Materials Physics (CAMP), Denmark Technical University, Lyngby, Denmark; with local extensions by L. Bengtsson.
[37] G. Kresse and J. Furthmüller, Phys. Rev. B **54**, 11 169 (1996).
[38] D. Vanderbilt, Phys. Rev. B **41**, 7892 (1990).
[39] G. Kresse and J. Hafner, J. Phys.: Condens. Matter **6**, 8245 (1994).
[40] M.C. Payne, M.P. Teter, D.C. Allan, T.A. Arias, and J.D. Joan-

nopoulos, Rev. Mod. Phys. **64**, 1045 (1992).
[41] H.J. Monkhorst and J.D. Pack, Phys. Rev. B **13**, 5188 (1976).
[42] F. Ercolessi and J. Adams, Europhys. Lett. **26**, 583 (1994).
[43] I.J. Robertson, V. Heine, and M.C. Payne, Phys. Rev. Lett. **70**, 1944 (1993).
[44] M.P. Allen and D.J. Tildesley, *Computer Simulation of Liquids* (Oxford Science, Oxford, 1987).
[45] T.R. Mattsson and A.E. Mattsson, Phys. Rev. B **66**, 214110 (2002).
[46] Y. Mishin, M.R. Sørensen, and A.F. Voter, Philos. Mag. A **81**, 2591 (2001).
[47] N. Sandberg, B. Magyari-Köpe, and T.R. Mattsson, Phys. Rev. Lett. **89**, 065901 (2002).
[48] S. Kurth, J.P. Perdew, and P. Blaha, Int. J. Quantum Chem. **75**, 889 (1999).
[49] U. Klemradt, B. Drittler, T. Hoshino, R. Zeller, P.H. Dederichs, and N. Stefanou, Phys. Rev. B **43**, 9487 (1991).
[50] P.A. Korzhavyi, I.A. Abrikosov, B. Johansson, A.V. Ruban, and H.L. Skriver, Phys. Rev. B **59**, 11 693 (1999).
[51] K.M. Ho and K.P. Bohnen, Phys. Rev. B **32**, 3446 (1985).
[52] Sometimes the ''divacancy association entropy'' $\Delta S_{2V} \equiv S^{F}_{2V} - 2S^{F}_{1V}$ is defined, instead of the binding entropy.
[53] P. Erhart, P. Jung, H. Schult, and H. Ullmaier, in *Atomic Defects in Metals*, edited by H. Ullmeier, *Landolt-Börnstein, New Series*, Group III, Vol. 25 (Springer-Verlag, Berlin, Heidleberg, 1991).